Hindawi
Journal of Chemistry
Volume 2020, Article ID 8036961, 13 pages
https://doi.org/10.1155/2020/8036961

*Research Article*

# Fabrication of Ceramsite Adsorbent from Industrial Wastes for the Removal of Phosphorus from Aqueous Solutions

**Yue Yin**,[1] **Gaoyang Xu**,[1] **Linlin Li**,[1] **Yuxing Xu**,[1] **Yihan Zhang**,[1] **Changqing Liu**,[1] **and Zhibin Zhang**[2]

[1]*School of Environmental and Municipal Engineering, Qingdao University of Technology, Qingdao 266033, China*
[2]*School of Municipal and Environmental Engineering, Shandong Jianzhu University, Jinan 250101, China*

Correspondence should be addressed to Changqing Liu; lcqlfyqut@126.com

Received 4 July 2020; Revised 21 September 2020; Accepted 6 October 2020; Published 26 October 2020

Academic Editor: Leonardo Palmisano



A more applicable adsorbent was fabricated using industrial wastes such as red mud, fly ash, and riverbed sediments. The heavy metal inside the raw materials created metal hydroxy on the adsorbent surface that offered elevated adsorption capacity for phosphorus. The required equilibrium time for the adsorption is only 10 min. The theoretical maximum adsorption capacity of the adsorbent was 9.84 $mg \cdot g^{-1}$ inferred from the Langmuir adsorption isotherm. Higher solution pH favored phosphorus adsorption. Kinetics study showed that the adsorption could be better fitted by the pseudo-second-order kinetic model. The presence of coexisting anions had no significant adverse impact on phosphorus removal. The speciation of the adsorbed phosphorus indicated that the adsorption to iron and aluminum is the dominating adsorption mechanism. Moreover, a dynamic adsorption column experiment showed that, under a hydraulic time of 10 min, more than 80% of the phosphorus in the influent was removed and the surplus phosphorus concentration was close to 0.1 $mg\,L^{-1}$. The water quality after adsorption revealed its applicability in real treatment. Consequently, the adsorbent synthesized from industrial wastes is efficient and applicable due to the high efficiency of phosphorus removal and eco-friendly behavior in solutions.

## 1. Introduction

Wastewater discharging to water bodies such as rivers and lakes will deteriorate the water quality. Phosphorus is one of the most influential pollutants in wastewater, and excessive phosphorus leads to eutrophication [1]. Eutrophication has become a serious environmental problem worldwide as it is accompanied by rapid overgrowth of algae which will deplete the oxygen in the water and suffocate the aquatic animals [2, 3]. In addition, phosphorus scarcity is another troublesome issue, mined rock phosphate is the major source of phosphorus, and the existing mine rock phosphate will become exhausted in less than 100 years [4]. In wastewater treatment, most of the technologies are designed only followed by the wastewater discharge threshold without the purpose of phosphorus recovery, but in China, approximately 1378 t of phosphorus was discharged directly without any recycling in 2018 (http://www.mohurd.gov.cn/csjs/xmzb/index.htm). In order to recover the phosphorus for reuse simultaneously, it is urgent to develop new technologies that could remove the phosphorus in the wastewater completely and recover the phosphorus resource. The application of proper adsorbents could be one of the solutions to meet the requirements [5–7]. Several reports have investigated the ability of phosphorus removal and recovery of different adsorbents [8, 9]. For example, rare earth element lanthanum and graphene were used as materials of adsorbents because of their high phosphate attention capability [10, 11]. The calculated adsorption capacity was higher than most of the low-cost adsorbents. However, the cost of the adsorbents such as lanthanum-based and graphene-based adsorbents is not mentioned, but considering its high-price raw materials and complicated fabrication synthesis process, the cost will be unacceptable in wastewater treatment. Furthermore, the spent adsorbents need further disposal. Consequently, these disadvantages hinder practical applications.

In the past decades, the adsorbents made from hazardous materials have gained great concerns because of its removal capacity of anionic pollutants and low cost. Many literature studies have reported the use of fly ash [12], red mud [13], tailings [14], and blast furnace slag [15] to manufacture ceramsite adsorbents to remove phosphorus from aqueous solutions. Wang et al. [12] reported a phosphorus adsorption comparison among red mud, fly ash, ferric-alum water treatment residual, and their modified materials, and the results demonstrate that the iron-modified materials were better than HCl-modified materials, and ferric-alum water treatment residual was better than red mud and fly ash. Another research by Tangde et al. [16] investigated the phosphate adsorption onto activated red mud, and the results indicated that the maximum adsorption capacity of activated red mud was 112.36 mg·g$^{-1}$ at optimum pH 2. However, to the best of the authors' knowledge, no literature is mixing contaminated riverbed sediments with red mud and fly ash to fabricate ceramsite adsorbent. For one thing, the riverbed sediments are in a great amount of silicon which is the main component for producing ceramsite, the clay used in the past is exhausting in earth, and replacing clay with riverbed sediments can be prompted in construction and water treatment works [17]. In addition, the incineration process will stabilize the heavy metal inside the riverbed sediments and reduce the heavy metal leaching which favored its practical application.

In Shandong province, China, the heavy industry accounts for a large proportion which caused too much industrial wastes such as red mud and fly ash [18]. On the other hand, river pollution is not peculiar in Shandong, and many rivers were polluted at different levels. With the effort the government made in recent years, the water in rivers is now less polluted or unpolluted; nevertheless, the sediments on the riverbed have been compromised due to long-term contamination. This large amount of the sediments cannot be treated only by in situ solidification because most of the sediments are active and unable to be repaired easily. In this study, fly ash and red mud were added into contaminated riverbed sediments to fabricate ceramsite. Hence, using these waste materials to manufacture ceramsite will stabilize the pollutants inside, effectively lower the ecological risk of the waste, and utilize the elements present in the waste to strengthen the adsorption capacity.

The objective of this study is to investigate the feasibility of "use the waste to treat the waste," and in other words, the adsorption capacity of ceramsite made from the combination of red mud, fly ash, and contaminated riverbed sediments. To meet the real application, the adsorption time in this study was set at 10 minutes while the equilibrium time in other research studies ranged from 0.5 to 48 hours. Also, the pH in every experiment (except for pH study) was set at 7 to be more representative. Kinetic and adsorption isotherm were investigated to analyze the adsorption process, along with the effect of pH, coexisting anions, and dosage. The speciation of the adsorbed phosphorus was further investigated to characterize the adsorption mechanism. For the application of ceramsite, the real wastewater adsorption, dynamic column adsorption, and desorption experiments were also elucidated.

## 2. Materials and Methods

*2.1. Materials.* All chemicals used in this study were of analytical grade purchased from Sinopharm Chemical Reagent Co., Ltd. All data were triplicated, the values were averaged, and the relative standard deviations were below 8% in all values. The red mud and fly ash were obtained from the industry in Shandong province. The heavy metal contaminated riverbed sediment was sampled from a heavy-polluted river located in Shandong province. The chemical and mineral compositions of the raw materials used in this research are given in Table 1 and Figure 1, respectively. Deionized water was used in this study.

*2.2. Synthesis of Ceramsite.* Raw materials were air-dried for 10 days to remove moisture and then ground to pass a 48-mesh sieve. The riverbed sediment, fly ash, red mud, and sawdust were mixed at 5 : 3 : 1 : 1 (w/w) and deionized water was added (20 wt%). The mixture was ground into pellets (diameter: 8–10 mm) and dried at 105°C for 4 hours in an oven. The origin pellets were incinerated in a muffle furnace at 900°C for 1 hour with a ramp at 10°C min$^{-1}$. The achieved ceramsite was cooled naturally, ground to pass 20-mesh sieve (~1.27 mm), and stored in a desiccator for future use.

*2.3. Characterization of Ceramsite.* The chemical composition was determined by X-ray fluorescence spectroscopy (XRF-1800, SHIMADZU). Mineralogical detection was carried out using X-ray diffraction (XRD, Rigaku) using Cu radiation (45 kV, 40 mA). The surface morphologies were examined by scanning electron microscopy (SU8000, Hitachi). BET surface area was detected by Micromeritics ASAP2460. The point of zero charge of ceramsite made from industrial wastes was tested according to the solid addition method [19]. Briefly, each flask contained 0.1 g ceramsite and 100 mL 0.01 M $KNO_3$ solution with pH between 2 and 10 and was shaken for 10 min to reach equilibrium. The initial pH was adjusted by using 0.1 M HCl and 0.1 M NaOH, and the final pH of the solutions was measured. The change of the pH value (before and after shaking) was designated as ΔpH which was plotted against initial pH, and the pH at the point of zero charge (pHpzc) value was at the initial pH value where ΔpH is equal to zero (where the curve intersects the $X$-axis) [20].

*2.4. Static Adsorption Methods.* To study equilibrium phosphorus adsorption capacity, 0.5 g ceramsite was added into a conical flask with 50 mL of a phosphate concentration varying from 1 to 20 mg L$^{-1}$. The mixture was shaken at 120 rpm for 10 min in a thermostatic shaker. After that, the mixed solution was filtered through a 0.45 $\mu$m membrane and the phosphate concentration was detected using the molybdenum-blue complex method. The phosphorus adsorption capacity of ceramsite ($q_e$ (mg g$^{-1}$)) and the removal

Table 1: Chemical compositions of raw materials (% by mass).

| | $SiO_2$ | $Al_2O_3$ | CaO | $Fe_2O_3$ | $SO_3$ | $Na_2O$ | $TiO_2$ |
|---|---|---|---|---|---|---|---|
| Riverbed sediment | 56.58 | 14.52 | 13.29 | 6.68 | 1.00 | 1.02 | 0.88 |
| Red mud | 20.86 | 22.40 | 3.73 | 36.00 | 0.52 | 10.46 | 5.00 |
| Fly ash | 1.55 | 0.72 | 44.60 | 0.23 | 52.47 | 0.23 | ND |

ND = not detected.

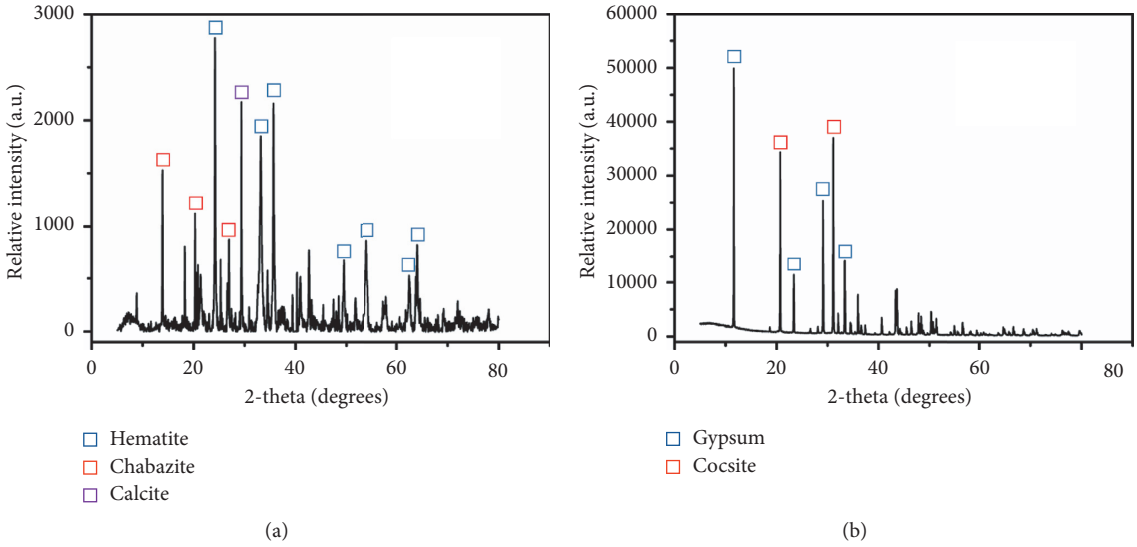


Figure 1: XRD spectra of (a) red mud and (b) fly ash.

rate of the phosphorus ($R$(%)) were calculated by the following equations:

$$q_e = \frac{(C_0 - C_e)}{a}, \quad (1)$$

$$R = \frac{(C_0 - C_e)}{C_0} \times 100\%, \quad (2)$$

where $C_0$ (mg·L$^{-1}$) is the initial phosphorus concentration, $C_e$ (mg·L$^{-1}$) is the phosphorus concentration at equilibrium, and $a$ (g·L$^{-1}$) is the adsorbent dosage.

For kinetics studies, 0.5 g ceramsite was added into phosphate solution (concentration = 10, 5, and 2 mg L$^{-1}$), and the mixture was shaken for different times (10 s–600 s) and tested as previously mentioned. For the effect of pH on phosphorus adsorption, phosphorus solutions were prepared at different initial pH conditions using 0.1 M HCl or 0.1 M NaOH (phosphorus concentration = 10 mg·L$^{-1}$ and adsorbent dosage = 1 g·L$^{-1}$) and shaken for 10 min at 25°C. In the dosage effect study, different adsorbent dosages were applied from 0.5 to 10 g·L$^{-1}$, mixing with phosphorus solutions of 50 mg·L$^{-1}$ and shaking for 10 min. To determine the effect of coexisting anions on phosphorus adsorption, the competing coexisting anions such as $Cl^-$, $F^-$, $SiO_3^{2-}$, and $SO_4^{2-}$ were added.

There are three kinds of phosphorus adsorbed on the adsorbents, namely, physically adsorbed phosphorus (phys-P), Fe/Al adsorbed phosphorus (Fe/Al-P), and Ca/Mg adsorbed phosphorus (Ca/Mg-P). To determine the speciation of the phosphorus adsorbed on the ceramsite, a modified sequential extraction procedure was used based on [21] after equilibrium (experimental condition: 10 min, 120 rpm, initial phosphorus concentration = 20 mg·L$^{-1}$, and adsorbent dosage = 5 g·L$^{-1}$). To be specific, the extraction procedure is shown in Table 2.

For recyclability of the spent adsorbent, different solutions were prepared to conduct desorption experiments including 0.1 M NaCl, 0.1 M $Na_2CO_3$, 0.1 M NaOH, 0.1 M HCl, and 0.1 M $H_2SO_4$. The experiment conditions were as follows: 10 g·L$^{-1}$ adsorbent, 50 mg·L$^{-1}$ phosphorus, 10 min, and 120 rpm. For real adsorption applications, water samples were collected from different places such as water treatment plants, wastewater treatment plants, parks, river, and city runoff. Unless otherwise stated, the pH of all phosphate solutions used in this study was adjusted to 7.

*2.5. Dynamic Column Adsorption.* Dynamic adsorption was conducted using laboratory-scale adsorption columns. The columns were made from polymethyl methacrylate with an inner diameter of 30 mm and a height of 100 mm. The column was packed with 20 g ceramsite with a functional volume of 50 ml. The effluent was prepared by dissolving $KH_2PO_4$ with deionized water to achieve different initial concentrations, and the HRT was maintained at 10 min.

Table 2: Extraction procedure for different speciation of phosphorus.

| Step | Method | Speciation |
|---|---|---|
| 1 | 1 g spent adsorbent added to 25 ml 1 M $NH_4Cl$, stirring for 1 h at 120 rpm (25°C) | Phys-P |
| 2 | Residual adsorbent added to 25 ml 0.1 M NaOH, stirring for 1 h at 120 rpm (25°C) | Fe/Al-P |
| 3 | Residual adsorbent added to 25 ml 0.5 M HCl, stirring for 1 h at 120 rpm (25°C) | Ca/Mg-P |
| 4 | Subtracting above 3 speciation phosphorus from equilibrium phosphorus amount | Loss-P |

## 3. Results and Discussion

*3.1. Characterization of Ceramsite.* XRD patterns of the raw materials and the adsorbent before and after adsorption are given in Figures 1 and 2. As from Figure 1(a), the crystalline phases of the raw red mud are identified as hematite, chabazite, and calcite. Figure 1(b) shows that the main mineral compositions of fly ash are gypsum and coesite. The iron, aluminum, silicon, and calcium present in the red mud and fly ash support the structure of the adsorbent and function as the major activated site to adsorb phosphorus. The XRD pattern of adsorbent before and after adsorption is depicted in Figure 2, and it can be seen that the adsorbent has a stable crystalline structure comparing to raw materials. Additionally, no obvious change is observed in the XRD pattern after adsorption indicates its great stability for phosphorus adsorption in aqueous solutions.

Figure 3 shows the morphology of ceramsite adsorbent with SEM which confirms the porous surface of the adsorbent. This heterogeneous surface will increase the adsorption capacity due to its higher specific surface area; meanwhile, porous surface will intercept the pollutants more easily and facilitate the adsorption process. The BET surface area of this adsorbent was 12.89 $m^2 \cdot g^{-1}$ which favors its adsorption, and the average pore size is 15.96 nm.

The FTIR spectrum of ceramsite adsorbent is given in Figure 4. The broad band at 3398 $cm^{-1}$ and a weak peak at 1633 $cm^{-1}$ of ceramsite adsorbent are due to the stretching vibrations of surface -OH or water [22]. Further, the peaks at 1011 $cm^{-1}$ and 1077 $cm^{-1}$ are related to the Fe-OH and Si-O, respectively, which are the fundamental groups for the adsorption of phosphorus in this study [23, 24]. The band at 578.7 $cm^{-1}$ pertains to symmetric stretching vibrations of Fe-O in crystalline lattice of $Fe_3O_4$ [25].

*3.2. Static Adsorption Studies*

*3.2.1. Adsorption Isotherms.* The adsorption isotherm data are given in Table 3. The maximum phosphorus adsorption capacity of ceramsite is achieved using different initial phosphorus concentrations at different temperatures. The isotherm data are shown in Figure 5 together with the data fitting by Langmuir isotherm. As from Figure 5(a), the increase of the environment temperature cannot improve the adsorption capacity under low phosphorus concentration, whereas a prominent increase was observed under high phosphorus concentration, indicating an endothermic nature of the adsorption process. This nature was not significant under low phosphorus concentration due to sufficient

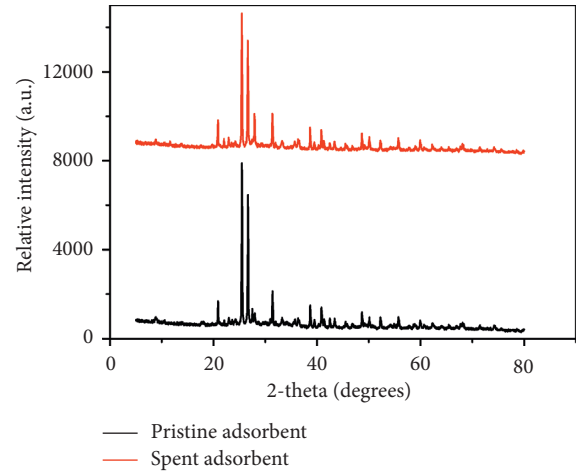


Figure 2: XRD spectra of adsorbent before and after adsorption.

adsorption. The highest phosphorus adsorption capacities are 9.18, 10.56, and 11.61 $mg \cdot g^{-1}$ achieved at 25, 35, and 45°C. The Langmuir model and Freundlich isotherm are used to fit the adsorption data, and the isotherm equations are expressed as follows [7, 26]:

$$\frac{C_e}{q_e} = \frac{1}{K_L q_{\max}} + \frac{1}{q_{\max}} C_e, \qquad \ln q_e = \ln K_F + \frac{1}{n} \ln C_e, \tag{3}$$

where $C_e$ ($mg \cdot L^{-1}$) is the phosphorus concentration at equilibrium, $q_e$ is the adsorption capacity. $q_{\max}$ ($mg \cdot g^{-1}$) represents the theoretical maximum adsorption capacity, $K_L$ ($L \cdot mg^{-1}$) is the equilibrium constant related to adsorption energy, $K_F$ ($mg \cdot g^{-1}$) is the Freundlich adsorption capacity, and the $n$ is the Freundlich constant.

As shown in Table 3, the experiment data are fitted well at every control temperature with the Langmuir isotherm model with higher correlation coefficients but poorly with Freundlich isotherm, and this means that the adsorption of the phosphorus onto the ceramsite is limited to monolayer coverage [27]. The theoretical maximum adsorption capacities calculated from the Langmuir model are 9.84, 11.52, and 13.05 $mg \cdot g^{-1}$, respectively, at 25, 35, and 45°C, which is at the medium level of the previously reported research studies listed in Table 4; however, the adsorption time in this study is only 10 minutes which is less than most of the other research studies. We thought the time as a vital operating parameter in adsorption because the long adsorption duration is impossible in wastewater treatment due to a large cost.

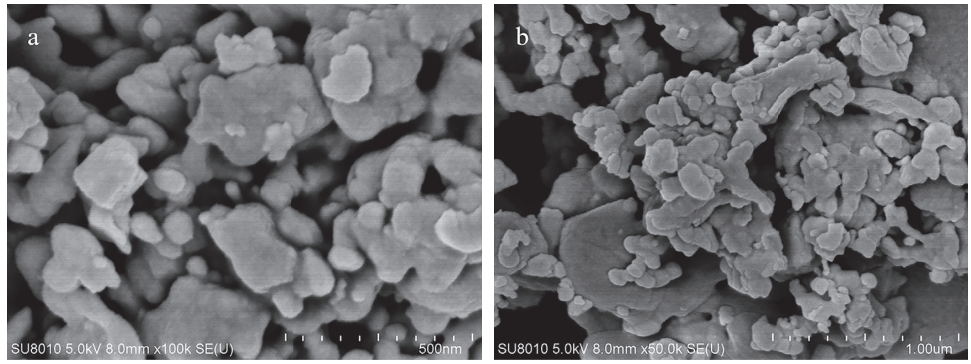


Figure 3: Morphology of adsorbent surface: (a) ×100000 and (b) ×50000.

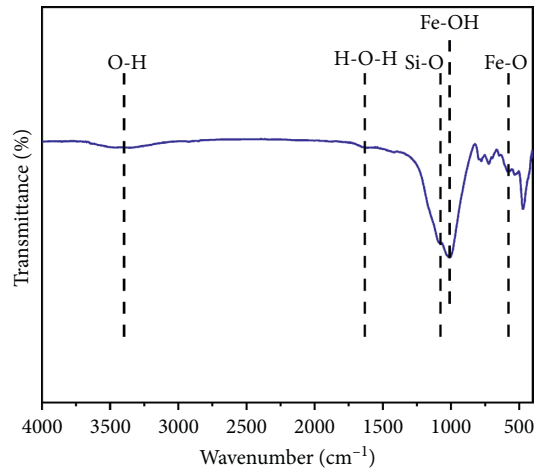


Figure 4: FTIR spectrum of ceramsite adsorbent.

Table 3: Langmuir and Freundlich isotherm constants.

| Temperature (°C) | Langmuir | | | Freundlich | | |
|---|---|---|---|---|---|---|
| | $q_{max}$ (mg·g$^{-1}$) | $K_L$ (L·mg$^{-1}$) | $R^2$ | $K_F$ (mg·g$^{-1}$) | $n$ | $R^2$ |
| 25 | 9.84 | 1.35 | 0.9871 | 4.35 | 2.30 | 0.6525 |
| 35 | 11.52 | 1.37 | 0.9847 | 5.03 | 2.09 | 0.7316 |
| 45 | 13.05 | 1.18 | 0.9855 | 5.31 | 1.82 | 0.8469 |

The essential feature of the Langmuir isotherm can be presented in terms of the constant, $R_L$, which is expressed as follows [28]:

$$R_L = \frac{1}{1 + K_L C_0}. \quad (4)$$

The value of $R_L$ represents whether the phosphorus adsorption is favorable or unfavorable. If $0 < R_L < 1$, the adsorption is favorable under this initial concentration, and otherwise, it is unfavorable. All $R_L$ values under different conditions in this study are in the range of 0-1 (Table 5), which means the adsorption of the phosphorus onto the ceramsite proceeds in a favorable direction [29].

*3.2.2. Adsorption Kinetics.* Figure 6(a) shows the time dependence of phosphorus concentration at an initial adsorbent dosage of 0.5 g·L$^{-1}$ and different phosphorus concentrations varying from 2 to 10 mg·L$^{-1}$. The phosphorus concentration declines pronouncedly at the first 60 seconds and slowly afterward, following by a plateau at 10 min. At first, the active sites on the surface of the adsorbent were sufficient which caused a rapid adsorption, and after some of the adsorption sites were occupied by the phosphate, the adsorption speed for the remaining sites will be compromised by the occupied sites nearby and the decreasing phosphate concentration in the solutions. The addition of the dosage was 0.5 g·L$^{-1}$ which caused not sufficient adsorption for phosphorus. Notably, the equilibrium concentration of initial 10 mg·L$^{-1}$ is close to 2 mg·L$^{-1}$, which means the phosphorus removal capacity will be improved with higher initial concentration. The adsorption kinetics are also fitted to achieve a better understanding of phosphorus adsorption behavior (Figures 6(b) and 6(c)). In this work,

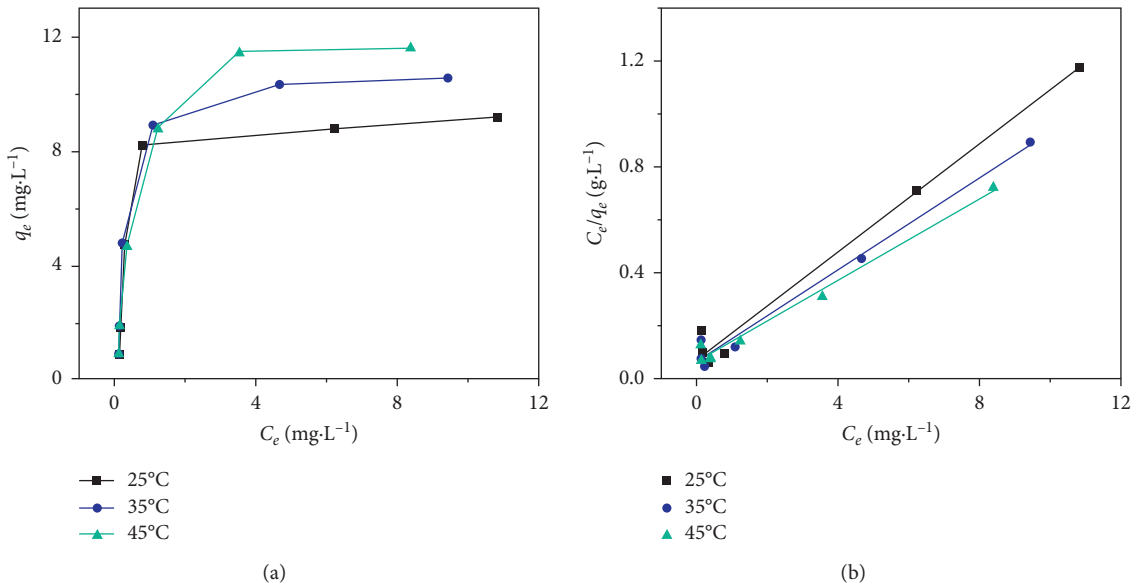


Figure 5: (a) Adsorption of phosphorus onto ceramsite; (b) Langmuir model fitting (pH = 7, $t$ = 10 min, adsorbent dosage = 1 g·L$^{-1}$, and 120 rpm).

Table 4: Removal capacity comparison of different phosphorus adsorbents.

| Adsorbent | Experimental conditions | | | $q_e$ (mg·g-1) | Reference |
|---|---|---|---|---|---|
| | Adsorbent dosage (g·L$^{-1}$) | Time (hours) | pH | | |
| Mg-loaded biochar | 1 | 4 | 7 | 31.15 | [30] |
| Modified bauxite residue | 40 | 24 | NA | 0.35–2.73 | [31] |
| Fe-loaded ceramic adsorbent | 1 | 3 | 7 | 18.48 | [32] |
| Acid-engineered pumice | 2 | 0.5 | 5–7 | 9.74 | [33] |
| Granular mesoporous ceramic | 10 | 24 | 4.0–12.0 | 5.96 | [34] |
| Lithium silica fume | 2 | 6 | 7 | 24.10 | [35] |
| Wasted low-grade iron ore | 10 | 1 | 5.6 | 11.44 | [36] |
| Industrial waste ceramsite | 1 | 0.167 | 7 | 9.84 | This study |

Table 5: The $R_L$ values at different initial phosphorus concentrations.

| Temperature (°C) | $R_L$ values at different initial phosphorus concentrations | | | | | |
|---|---|---|---|---|---|---|
| | 1 mg·L$^{-1}$ | 2 mg·L$^{-1}$ | 5 mg·L$^{-1}$ | 10 mg·L$^{-1}$ | 15 mg·L$^{-1}$ | 20 mg·L$^{-1}$ |
| 25 | 0.43 | 0.27 | 0.13 | $6.90\times10^{-2}$ | $4.71\times10^{-2}$ | $3.57\times10^{-2}$ |
| 35 | 0.42 | 0.27 | 0.13 | $6.79\times10^{-2}$ | $4.63\times10^{-2}$ | $3.51\times10^{-2}$ |
| 45 | 0.46 | 0.30 | 0.15 | $7.83\times10^{-2}$ | $5.36\times10^{-2}$ | $4.08\times10^{-2}$ |

the pseudo-first-order and pseudo-second-order model are used to fit the adsorption data, and the equations are as follows [37, 38]:

$$\ln(q_e - q_t) = \ln q_e - K_1 t,$$
$$\frac{t}{q_t} = \frac{1}{K_2 q_e^2} + \frac{t}{q_e}, \quad (5)$$

where $q_e$ and $q_t$ are the amount of phosphorus adsorbed per unit mass adsorbent at equilibrium and at different time $t$, respectively. $K_1$ (min$^{-1}$) and $K_2$ (g·mg$^{-1}$·min$^{-1}$) are the kinetic rate constants.

All the experimental data fit the pseudo-second-order model well with higher correlation coefficients as shown in Table 6. It is also notable that the experimental $q_e$ agrees with the calculated $q_e$ derived from the pseudo-second-order model, and this also demonstrates that the phosphorus adsorption onto ceramsite followed the pseudo-second-order model which means that the adsorption might be the rate-limiting step [39].

*3.2.3. Effect of Operational Conditions.* The adsorption of phosphorus onto ceramsite was highly affected by the initial pH condition because it changed the surface charge on the

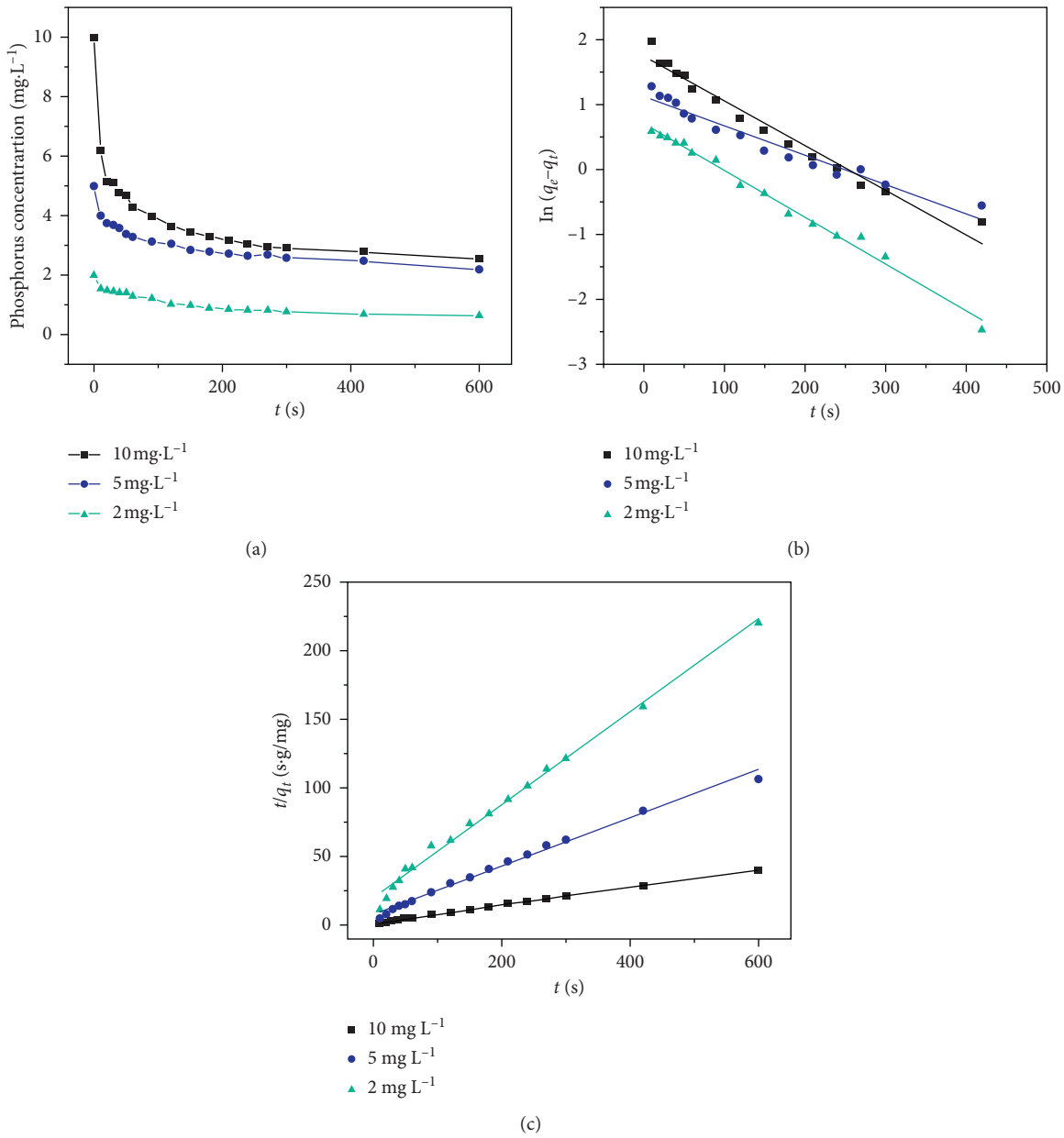


Figure 6: (a) Adsorption kinetics of phosphorus onto ceramsite; (b) pseudo-first-order model fitting; (c) pseudo-second-order model fitting (pH = 7, $t$ = 10 min, adsorbent dosage = 0.5 g·L$^{-1}$, 120 rpm, and 25°C).

Table 6: Pseudo-first-order and pseudo-second-order kinetics constants.

| Phosphorus concentration (mg·L$^{-1}$) | Experimental value $q_e$ (mg·g$^{-1}$) | Pseudo-first-order model | | | Pseudo-second-order model | | |
|---|---|---|---|---|---|---|---|
| | | $K_1$ (min$^{-1}$) | $q_e$ (mg·g$^{-1}$) | $R^2$ | $K_2$ (g·mg$^{-1}$·min$^{-1}$) | $q_e$ (mg·g$^{-1}$) | $R^2$ |
| 2 | 2.72 | $7.20 \times 10^{-3}$ | 2.03 | 0.9901 | $5.96 \times 10^{-3}$ | 2.94 | 0.9931 |
| 5 | 5.63 | $4.51 \times 10^{-3}$ | 3.10 | 0.9526 | $4.10 \times 10^{-3}$ | 5.70 | 0.9918 |
| 10 | 14.89 | $6.85 \times 10^{-3}$ | 5.73 | 0.9687 | $3.37 \times 10^{-3}$ | 15.17 | 0.9991 |

adsorbents, and the pH condition can be considered as one of the most influential factors in adsorption behavior [40]. To investigate the pH dependence of phosphorus adsorption capacity, adsorption was conducted under different pH conditions varying from 1 to 13 with an initial concentration of 10 mg L$^{-1}$ and adsorbent dosage of 1 g·L$^{-1}$. As shown in Figure 7, the adsorption capacity was on the rise following the initial pH from 1 to 5, achieving the highest adsorption

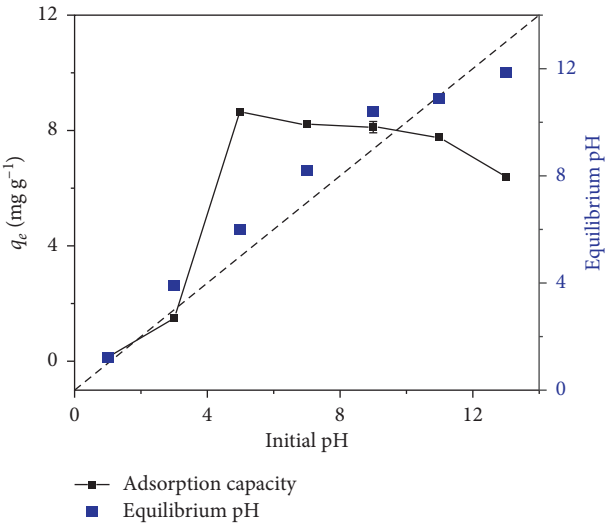


Figure 7: Effect of pH on the phosphorus adsorption behavior and final pH after reaching equilibrium ($t$ = 10 min, adsorbent dosage = 1 g·L$^{-1}$, 120 rpm, initial phosphorus concentration = 10 mg·L$^{-1}$, and 25°C).

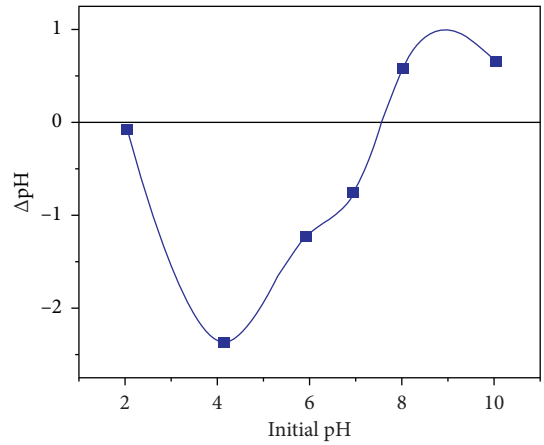


Figure 8: Point of zero charge of ceramsite.

capacity at pH = 5, and after that, a negative influence of pH was observed. The same tendency was also observed in other research studies but with higher adsorption capacity in low pH conditions [12]. This result may be because the pH has a great influence on the phosphorus species and ceramsite surface charge. As it is well known the phosphorus species were greatly influenced by pH, under 25°C condition, the predominated phosphorus species were $H_2PO_4^-$, $HPO_4^{2-}$, and $PO_4^{3-}$ with the pH starting from 2.1, 7.2, and 12.3, respectively, resulting in more negatively charged phosphorus species with the increase of pH [12]. The point of zero charge of pH is plotted in Figure 8 which was in the pH range from 7 to 8, with lower pH than pHpzc, the surface of the adsorbent was positively charged, and on the contrary, the surface was negatively charged with higher pH than pHpzc. Hence, when the surrounding pH was lower than pHpzc, with the decrease of pH, the amount of the positively charged sites on the ceramsite increased. However, the adsorption behavior under low pH was compromised which may be owing to the less negative form of phosphorus ($H_3PO_4$ and $H_2PO_4^-$), while with the increase of pH, the increased percentage of $HPO_4^{2-}$ built a strong bond with the Fe/Al surface resulting in better adsorption performance. Besides, the extremely low pH surrounding may disassemble the fraction of ceramsite which will release more anions into the solution competing with phosphorus. While under highly alkaline condition, the surface charge was highly negative which should have an adverse impact on phosphorus removal; however, the alkaline condition promoted the transformation of $HPO_4^{2-}$ to $PO_4^{3-}$ which is more active to form strong precipitation with iron and aluminum causing stable adsorption behavior under high alkaline condition. The pH-dependent adsorption curve indicated that the adsorption was inhibited under low pH (1–3) and stayed active afterward even at pH = 13. The solution pH was also measured after reaching equilibrium, presented as blue quadrates in Figure 7, and it was seen that the equilibrium pH increased slightly with initial pH ranging from 1 to 9 and decreased at highly alkaline conditions, which also can be used to demonstrate that negatively charged particles were released under the acid condition and compete with phosphorus anions.

For the investigation of the effect of dosage on phosphorus adsorption, the adsorption experiments were conducted with different dosage amounts ranging from 0.5 to 10 g·L$^{-1}$ in the presence of 50 mg·L$^{-1}$ initial phosphorus at 120 rpm for 10 min (Figure 9). The phosphorus adsorption rate significantly increased from 15.905% to 99.24% with increasing ceramsite dosage amount from 0.5 to 5 g·L$^{-1}$. The adsorption rate stayed constant after 5 g·L$^{-1}$ adsorbent with the effluent phosphorus concentration below 1.5 mg·L$^{-1}$. With the increase of the dosage amount, the active sites increased which can adsorb more phosphorus, leading to an inevitable increasing adsorption rate, and on the other hand, the phosphorus adsorption capacity in unit mass decreased from 15.905 to 0.995 mg g$^{-1}$ because, with the increase of adsorbents, the adsorption force of specific surface area got weakened [41]. It was seen from that, considering large initial phosphorus concentration, 5 g·L$^{-1}$ adsorbent was found to be an effective dosage.

Figure 10 presents the influence of the coexisting anions on the phosphorus adsorption including $Cl^-$, $F^-$, $SiO_3^{2-}$, and $SO_4^{2-}$ anions at different concentrations (20 and 100 mg·L$^{-1}$). The blue line in this figure represents the adsorption capacity without coexisting anions under the same experimental conditions, and as from the comparison, the influence of the anions in descending order was as follows: $SO_4^{2-}$, $SiO_3^{2-}$, $F^-$, and $Cl^-$. All four anions present in the solutions affected the phosphorus adsorption of ceramsite, but still, no remarkable impact was detected. From Figure 10, with 20 mg·L$^{-1}$ of coexisting anions, the phosphate removal rate achieved 99.31%, 99.12%, 98.89%, and 98.69% for $Cl^-$, $F^-$, $SiO_3^{2-}$, and $SO_4^{2-}$, respectively. Under higher concentration of coexisting anions (100 mg·L$^{-1}$), no significant decrease was detected. Sulfate, because iionic radii (2.3 Å) is similar to that of phosphate (2.38 Å) which will cause competitive adsorption, was the most influential anion

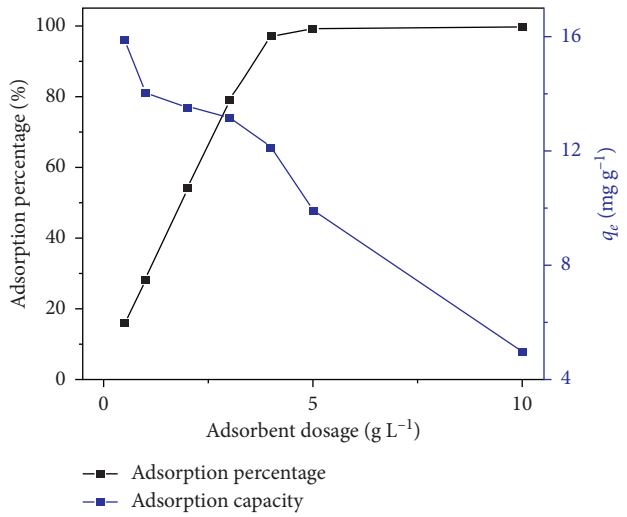


Figure 9: The effect of dosage on phosphorus adsorption (pH = 7, $t$ = 10 min, 120 rpm, initial phosphorus concentration = 50 mg·L$^{-1}$, and 25°C)

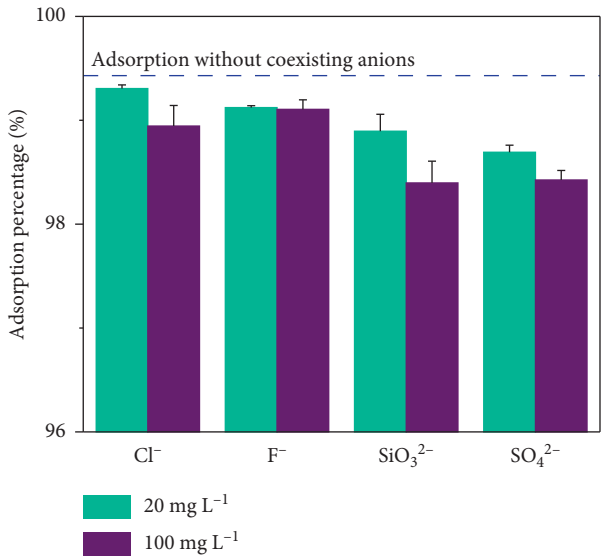


Figure 10: The effect of coexisting anions on phosphorus adsorption (pH = 7, $t$ = 10 min, adsorbent dosage = 2 g·L$^{-1}$, 120 rpm, initial phosphorus concentration = 10 mg·L$^{-1}$, and 25°C).

[42]. However, the detrimental effect caused by this competitive anion is negligible. This suggested that the adsorbent showed an exceptional anti-interference ability to other coexisting anions, proving the applicability of the adsorbent in complicated real water treatment.

*3.2.4. Speciation Analysis of Adsorbed Phosphorus.* To figure out the phosphorus adsorption mechanism of ceramsite, the speciation of the adsorbed phosphorus was distinguished using the sequential extraction procedure. From Figure 11, the Fe/Al-P was the dominating adsorption speciation, accounting for 85.91% of all the phosphorus adsorbed. This demonstrated that the adsorption of phosphorus was dominated by iron and aluminum which were the major

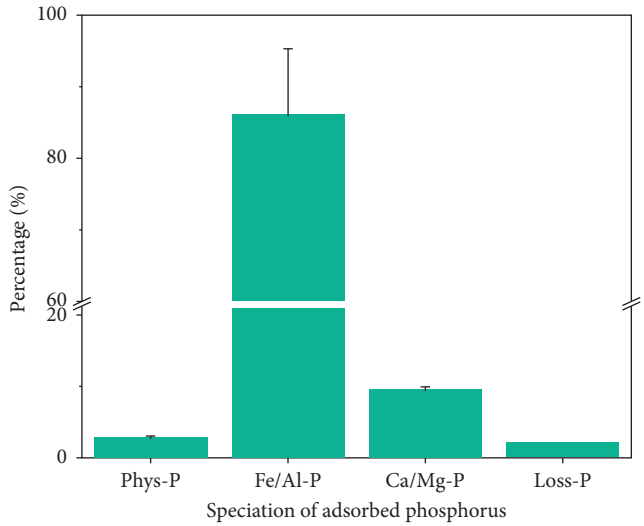


Figure 11: Speciation analysis of adsorbed phosphorus on ceramsite (pH = 7, $t$ = 10 min, adsorbent dosage = 2 g·L$^{-1}$, 120 rpm, initial phosphorus concentration = 10 mg·L$^{-1}$, and 25°C).

components of the red mud (36.00% and 22.40%, respectively, Table 1), and the phosphorus was precipitated on the surface of the ceramsite with iron and aluminum. In addition, 2.74% and 9.42% of phosphorus were adsorbed by physical adsorption and Ca/Mg adsorption, and the low percentage of Ca/Mg adsorption was due to the less active calcium in the ceramsite. Furthermore, only 1.93% of the total adsorbed phosphorus was not detected (loss-P); it indicated that all phosphorus was adsorbed at the surface of the ceramsite, and little phosphorus was removed with the dissolved iron or aluminum. Because of that, the phosphorus will remain on the surface of the ceramsite and can be desorbed using desorbing agents for the recovery of phosphorus.

*3.2.5. Desorption of Phosphorus.* Phosphorus desorption from the ceramsite is to help regenerate the adsorbents, and then the regenerated adsorbents can be used to adsorb phosphorus again. Preliminary research studies have indicated that sodium hydroxide, sodium bicarbonate, and sodium chloride can be used to regenerate the adsorbents [40, 43]. In this study, the desorption studies were conducted with different desorbing agents such as 0.1 M NaCl, 0.1 M $Na_2CO_3$, 0.1 M NaOH, 0.1 M HCl, and 0.1 M $H_2SO_4$, and phosphorus released from the adsorbents was measured to ensure the most functional desorbing agent. Unlike the preliminary research studies, the sodium hydroxide and sodium chloride barely desorbed the phosphorus from the surface, especially for sodium hydroxide, with less than 10% desorbing percentage. This might be caused by the reason that the majority of the phosphorus was adsorbed by iron and aluminum, and adding $OH^-$ will make the precipitation less soluble and difficult to break down. As from Figure 12, the best performance was achieved for 0.1 M HCl and 0.1 M $Na_2CO_3$ with 82.48% and 75.46% desorbing phosphorus of total phosphorus adsorbed, respectively. 0.1 M $H_2SO_4$ was

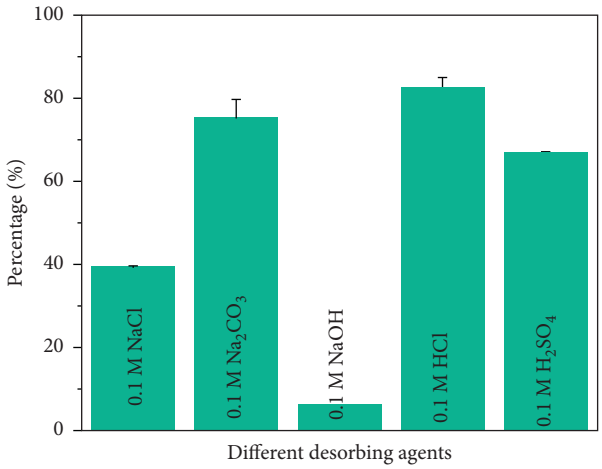


Figure 12: Percentage of phosphorus released from ceramsite using different desorbing agents (equilibrium: pH = 7, $t$ = 10 min, adsorbent dosage = 1 g·L$^{-1}$, 120 rpm, initial phosphorus concentration = 10 mg·L$^{-1}$, and 25°C).

also found to be very effective in the desorbing procedure. However, when testing the concentration of iron and aluminum in the solutions after desorption, higher concentration was observed with 0.1 M HCl and 0.1 M $H_2SO_4$, indicating the adsorbent was dissolved under the acidic solutions which caused desorption of phosphorus. The iron and aluminum concentrations after desorption were 0.53 and 1.23 mg L$^{-1}$ for 0.1 M HCl and 0.50 and 0.96 mg·L$^{-1}$ for 0.1 M $H_2SO_4$, respectively. Furthermore, nearly no iron/aluminum was detected after desorption using sodium carbonate. Consequently, sodium carbonate was chosen as the desorption agent for future use.

*3.2.6. Phosphorus Adsorption of Real Water Samples.* To truly investigate the feasibility of application for phosphorus removal using the ceramsite, the real water samples from different sources were collected and the detail of the samples is listed in Table 7. The water samples were collected from (a) water treatment plant, (b) wastewater treatment plant, (c) park, (d) river, and (e) runoff. The collected water samples initially contained phosphorus concentrations ranged from 0.04 to 3.23 mg·L$^{-1}$, and the COD ranged from 14 to 142. The results of phosphorus concentration before and after adsorption are shown in Figure 13. The phosphorus concentrations after adsorption decreased under 0.5 mg·L$^{-1}$ except for sample 6 which possessed more complicated water quality; however, it still adsorbed almost half of the phosphorus present in the water. This suggested that the application of ceramsite for real water treatment was feasible for low-contaminated aqueous solutions and also promising for complicated water samples if the appropriate adsorbent dosage was applied.

*3.3. Dynamic Column Adsorption.* Due to practical purposes, the column adsorption experiment was conducted in this research. Figure 14 shows the effect of inlet phosphorus concentrations on the effluent phosphorus concentration ($C$

Table 7: Details of collected water samples.

| Sample ID | pH | Temperature (°C) | COD (mg·L$^{-1}$) | $NH_4^+$-N (mg·L$^{-1}$) | $PO_4^{3-}$ (mg·L$^{-1}$) |
|---|---|---|---|---|---|
| 1 | 7.64 | 17.2 | 24 | 11.73 | 2.90 |
| 2 | 7.44 | 16.9 | 21 | 0 | 2.90 |
| 3 | 7.57 | 14.3 | 19 | 6.74 | 2.52 |
| 4 | 8.07 | 22.2 | 38 | 0.16 | 0.24 |
| 5 | 6.61 | 12.8 | 13 | 0.04 | 0.04 |
| 6 | 7.59 | 12.4 | 142 | 13.11 | 3.23 |
| 7 | 7.51 | 21.5 | 31 | 16.43 | 1.39 |
| 8 | 6.98 | 20.2 | 26 | 8.02 | 1.12 |

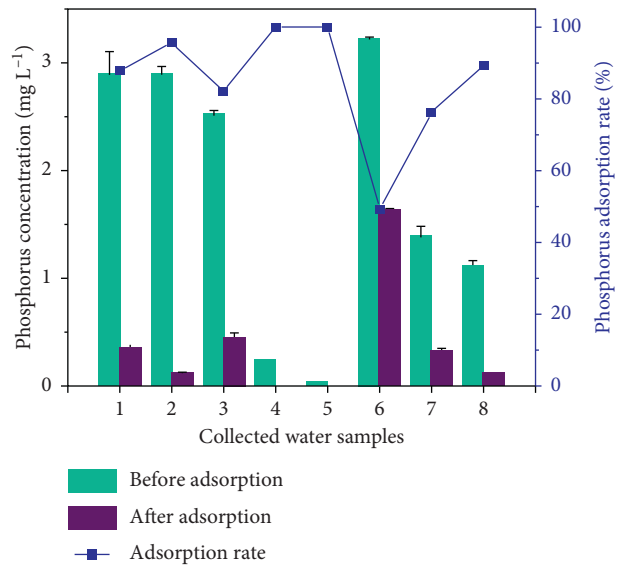


Figure 13: Phosphorus adsorption behavior of collected water samples (equilibrium: $t$ = 10 min, adsorbent dosage = 2 g·L$^{-1}$, 120 rpm, and 25°C).

is the effluent phosphorus concentration and $C_0$ is the initial phosphorus concentration). The results show that after approximately 30 and 40 minutes, with initial adsorbate concentration at 2 and 5 mg·L$^{-1}$, the phosphorus concentration in the effluent rises dramatically, indicating the adsorbent column has been broken through. Also, higher adsorbate concentration promotes the saturation time. After 50 minutes, the effluent phosphorus concentration is close to the influent phosphorus concentration (2 mg·L$^{-1}$) which indicates the adsorbent column is completely exhausted by the phosphorus. With initial phosphorus concentration at 2 mg·L$^{-1}$, the water samples collected prior to 34 minutes meet the threshold of the Chinese discharge standard of pollutants for municipal wastewater treatment plant (GB18918-2002), with the phosphorus concentration lower than 0.3 mg·L$^{-1}$. That is, the ceramsite adsorbent can remove 85% phosphorus using a fixed-bed column in a real application.

*3.4. Water Quality after Adsorption.* The water quality after adsorption was tested by ICP-MS, to ensure the safety of the ceramsite use in water treatment. Unlike other research

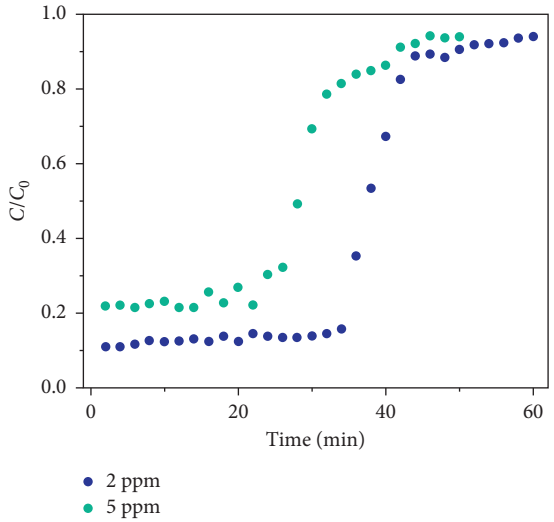


Figure 14: Removal of phosphorus by fixed-bed column (HRT = 10 min and dosage = 20 g).

Table 8: Trace metal element concentrations in the effluent (compared with leaching concentrations from raw materials).

| Metals (mg $L^{-1}$) | Water samples after column | | | Toxicity leaching tests | | | Maximum contaminant level |
|---|---|---|---|---|---|---|---|
| | 10 min | 20 min | 40 min | Red mud | Fly ash | Riverbed sediment | |
| As | 0.03 | 0.03 | 0.05 | 0.36 | 0.07 | 0.15 | 0.10 |
| Hg | ND | ND | ND | 0.01 | 0 | ND | 0.01 |
| Pb | ND | ND | ND | 0.01 | 0 | ND | 0.10 |
| Cd | 0.01 | 0.01 | 0.02 | 3.68 | 0.01 | 0.11 | 0.01 |
| Cr | 0.06 | 0.02 | 0.04 | 1.33 | 0.26 | ND | 0.10 |
| Fe | ND | ND | 0.09 | 0.96 | 0.29 | 0 | NM |
| Mg | 0.46 | 1.15 | 1.60 | 9.31 | 8.53 | 30.07 | NM |
| Al | 0.51 | 1.05 | 1.04 | 2.11 | 28.86 | 0.01 | NM |
| Ca | 3.87 | 18.31 | 8.12 | 382.97 | 427.73 | 605.03 | NM |
| Cu | 0.01 | 0.01 | 0.01 | 0.05 | 0.04 | 0.02 | 0.50 |
| Mn | ND | ND | 0.007 | 0.01 | 0.09 | 5.85 | 2.00 |
| Zn | 0.01 | 0.01 | 0.03 | 0.07 | 0.11 | 0.46 | 1.00 |

ND: not detected; NM: not mentioned.

studies, the objective of this work is to (1) treat the hazardous materials, (2) reuse them, and (3) ensure the feasibility for actual use but not for lab researches. Many research studies have investigated adsorbents with large adsorption capacity posing promising future; however, few of them studied the water quality after adsorption which is of great significance because the fundamental purpose of the adsorption treatment is to treat the water but not introduce more hazardous ions into the water. In addition, some of them may study the leaching toxicity, but the threshold standard they use is for the identification of hazardous materials but not for wastewater treatment standards. In this research, the water samples after 10 min, 20 min, and 40 min dynamic adsorption were tested to determine the metal concentrations, compared with the Chinese discharge standard of pollutants for municipal wastewater treatment plant (GB 18918–2002).

The concentrations of different metals after adsorption and the metal leaching concentrations of raw materials are shown in Table 8. In general, the concentrations after sintering decreased significantly compared with the leaching concentrations of raw materials, suggesting that the fabrication helped stabilize the metals inside the raw materials. Additionally, among the metals tested in this study, there are five metal pollutants listed as class I pollutants: As, Hg, Pb, Cd, and Cr. The measurement results showed that the As, Hg, Pb, and Cr concentrations of all water samples after adsorption column met completely the discharge standard of China. The Cd concentration after 40 minutes, however, exceeded 0.01 mg·$L^{-1}$ which will need further treatment. This may be caused by the large presence of cadmium inside the red mud (3.68 mg·$L^{-1}$ using TCLP test), and future fabrication should focus on the further stabilization of the cadmium. In the wastewater discharge standard, there are no specific limits for Fe, Mg, Al, and Ca elements; however, in this study, the concentrations were lowered to an unharmful level. Meanwhile, the remaining elements were within the discharge standard of pollutants for the wastewater treatment plant. Therefore, the adsorbent made in this research is relatively safe to use in wastewater treatment.

## 4. Conclusion

For the first time, the riverbed sediments, red mud, and fly ash were used as the main materials for ceramsite adsorbent fabrication. The adsorption capacity for phosphorus was investigated along with the mechanism study and preliminary application explore. Due to the iron and aluminum present in the raw materials, the adsorption capacity of ceramsite is up to 9.84 mg $g^{-1}$. The phosphorus adsorption onto ceramsite follows the Langmuir monolayer adsorption model and pseudo-second-order kinetic model. The adsorbent exhibited a great anti-interference ability to other anions simultaneously existing in the solutions; besides, the results of phosphorus adsorption from collected real water samples further suggest that the ceramsite adsorbent in this research can be effective across a wide range of conditions and suitable for different water environments. Moreover, it only takes 10 minutes for the adsorbent to reach equilibrium in the solutions which are far more rapid than most of the research studies; this greatly lowers the cost of the adsorption treatment if applying in treatment plant. Leaching toxicity of the ceramsite is below the wastewater discharge standard. In a word, this ceramsite prepared with industrial wastes is a low-cost, rapid, safe, and effective adsorbent to remove phosphorus from real water. To a certain content, the research has realized the purpose "use the waste to treat the waste". Further research should focus on improving the phosphorus adsorption capacity to remove more phosphorus by optimizing the preparing conditions. In addition, to avoid second pollution, the leachability of the ceramsite adsorbents needs to be controlled which will greatly promote the applicability of the adsorbents.

## Data Availability

The data used to support the findings of this study are available from the corresponding author upon request.

## Additional Points

A novel ceramsite adsorbent was prepared with contaminated sediment. Adsorbent showed rapid adsorption behavior and great adsorption capacity. The adsorbent can be used for real applications with no environmental influence.

## Conflicts of Interest

The authors declare that there are no conflicts of interest regarding the publication of this paper.

## Acknowledgments

This study was funded by the Major Science and Technology Innovation Project of Shandong Province (Grant no. 2018YFJH0902).

## References

[1] O. Axinte, I. S. Bădescu, C. Stroe, V. Neacsu, L. Bulgariu, and D. Bulgariu, "Evolution of trophic parameters from Amara lake," *Environmental Engineering and Management Journal*, vol. 14, no. 3, pp. 559–565, 2015.

[2] O. Eljamal, A. M. E. Khalil, Y. Sugihara, and N. Matsunaga, "Phosphorus removal from aqueous solution by nanoscale zero valent iron in the presence of copper chloride," *Chemical Engineering Journal*, vol. 293, pp. 225–231, 2016.

[3] Z. Yang, L. Liu, L. Zhao et al., "Preparation and evaluation of bis (diallyl alkyl tertiary ammonium salt) polymer as a promising adsorbent for phosphorus removal," *Journal of Environmental Sciences*, vol. 86, pp. 24–37, 2019.

[4] D. Cordell, J.-O. Drangert, and S. White, "The story of phosphorus: global food security and food for thought," *Global Environmental Change*, vol. 19, no. 2, pp. 292–305, 2009.

[5] S. Nazerdeylami and R. Zare-Dorabei, "Simultaneous adsorption of Hg2+, Cd2+ and Cu2+ ions from aqueous solution with mesoporous silica/DZ and conditions optimise with experimental design: kinetic and isothermal studies," *Micro & Nano Letters*, vol. 14, no. 8, pp. 823–827, 2019.

[6] F. Ramezani and R. Zare-Dorabei, "Simultaneous ultrasonic-assisted removal of malachite green and methylene blue from aqueous solution by Zr-SBA-15," *Polyhedron*, vol. 166, pp. 153–161, 2019.

[7] R. Zare-Dorabei, S. M. Ferdowsi, A. Barzin, and A. Tadjarodi, "Highly efficient simultaneous ultrasonic-assisted adsorption of Pb(II), Cd(II), Ni(II) and Cu (II) ions from aqueous solutions by graphene oxide modified with 2,2′-dipyridylamine: central composite design optimization," *Ultrasonics Sonochemistry*, vol. 32, pp. 265–276, 2016.

[8] P. G. Tratnyek and R. L. Johnson, "Nanotechnologies for environmental cleanup," *Nano Today*, vol. 1, no. 2, pp. 44–48, 2006.

[9] W. Qiao, H. Bai, T. Tang, J. Miao, and Q. Yang, "Recovery and utilization of phosphorus in wastewater by magnetic Fe3O4/Zn-Al-Fe-La layered double hydroxides(LDHs)," *Colloids and Surfaces A: Physicochemical and Engineering Aspects*, vol. 577, pp. 118–128, 2019.

[10] X. Li, A. H. Elgarhy, M. E. Hassan, Y. Chen, G. Liu, and R. ElKorashey, "Removal of inorganic and organic phosphorus compounds from aqueous solution by ferrihydrite decoration onto graphene," *Environmental Monitoring and Assessment*, vol. 192, no. 6, 2020.

[11] J. Liu, Q. Zhou, J. Chen, L. Zhang, and N. Chang, "Phosphate adsorption on hydroxyl-iron-lanthanum doped activated carbon fiber," *Chemical Engineering Journal*, vol. 215-216, pp. 859–867, 2013.

[12] Y. Wang, Y. Yu, H. Li, and C. Shen, "Comparison study of phosphorus adsorption on different waste solids: fly ash, red mud and ferric-alum water treatment residues," *Journal of Environmental Sciences*, vol. 50, pp. 79–86, 2016.

[13] S. Wang, H. M. Ang, M. O. Tadé, and R. Mud, "Novel applications of red mud as coagulant, adsorbent and catalyst for environmentally benign processes," *Chemosphere*, vol. 72, no. 11, pp. 1621–1635, 2008.

[14] L. Zeng, X. Li, and J. Liu, "Adsorptive removal of phosphate from aqueous solutions using iron oxide tailings," *Water Research*, vol. 38, no. 5, pp. 1318–1326, 2004.

[15] S. Yasipourtehrani and T. Evans, "Pyrometallurgical process for recycling of valuable materials and waste management:

valorisation applications of blast furnace slags," *Sustainable and Economic Waste Management*, vol. 9, pp. 1–12, 2019.

[16] V. M. Tangde, S. S. Prajapati, B. B. Mandal, and N. P. Kulkarni, "Study of kinetics and thermodynamics of removal of phosphate from aqueous solution using activated red mud," *International Journal of Environmental Research*, vol. 11, no. 1, pp. 39–47, 2017.

[17] J. L. Zou, G. R. Xu, and G. B. Li, "Ceramsite obtained from water and wastewater sludge and its characteristics affected by $Fe_2O_3$, CaO, and MgO," *Journal of Hazardous Materials*, vol. 165, no. 1–3, pp. 995–1001, 2009.

[18] P. LIU, H.-j. ZHAO, L.-l. WANG et al., "Analysis of heavy metal sources for vegetable soils from Shandong province, China," *Agricultural Sciences in China*, vol. 10, no. 1, pp. 109–119, 2011.

[19] A. E. Zidan, N. M. Hilal, A. A. Emam, and A. A. El-Bayaa, "Adsorption of barium and iron ions from aqueous solutions by the activated carbon produced from masot ash," *Life Science Journal*, vol. 10, no. 3, pp. 2011–2020, 2013.

[20] Z. Zhu, L. Li, H. Zhang, Y. Qiu, and J. Zhao, "Adsorption of Lead and cadmium on ca-deficient hydroxyapatite," *Separation Science and Technology*, vol. 45, no. 2, pp. 262–268, 2010.

[21] G. Cheng, Q. Li, Z. Su, S. Sheng, and J. Fu, "Preparation, optimization, and application of sustainable ceramsite substrate from coal fly ash/waterworks sludge/oyster shell for phosphorus immobilization in constructed wetlands," *Journal of Cleaner Production*, vol. 175, pp. 572–581, 2018.

[22] M. K. Sahu, S. Mandal, S. S. Dash, P. Badhai, and R. K. Patel, "Removal of Pb(II) from aqueous solution by acid activated red mud," *Journal of Environmental Chemical Engineering*, vol. 1, no. 4, pp. 1315–1324, 2013.

[23] Z. Cheng, F. Fu, D. D. Dionysiou, and B. Tang, "Adsorption, oxidation, and reduction behavior of arsenic in the removal of aqueous As(III) by mesoporous Fe/Al bimetallic particles," *Water Research*, vol. 96, pp. 22–31, 2016.

[24] A. Naga Babu, G. V. Krishna Mohan, K. Kalpana, and K. Ravindhranath, "Removal of fluoride from water using $H_2O_2$-treated fine red mud doped in Zn-alginate beads as adsorbent," *Journal of Environmental Chemical Engineering*, vol. 6, no. 1, pp. 906–916, 2018.

[25] I. Akin, G. Arslan, A. Tor, M. Ersoz, and Y. Cengeloglu, "Arsenic(V) removal from underground water by magnetic nanoparticles synthesized from waste red mud," *Journal of Hazardous Materials*, vol. 235-236, pp. 62–68, 2012.

[26] Y. Zhou, L. Luan, B. Tang et al., "Fabrication of Schiff base decorated PAMAM dendrimer/magnetic $Fe_3O_4$ for selective removal of aqueous Hg(II)," *Chemical Engineering Journal*, vol. 398, Article ID 125651, 2020.

[27] J. Febrianto, A. N. Kosasih, J. Sunarso, Y.-H. Ju, N. Indraswati, and S. Ismadji, "Equilibrium and kinetic studies in adsorption of heavy metals using biosorbent: a summary of recent studies," *Journal of Hazardous Materials*, vol. 162, no. 2-3, pp. 616–645, 2009.

[28] S. Meenakshi, C. S. Sundaram, and R. Sukumar, "Enhanced fluoride sorption by mechanochemically activated kaolinites," *Journal of Hazardous Materials*, vol. 153, no. 1-2, pp. 164–172, 2008.

[29] J. Niu, P. Ding, X. Jia, G. Hu, and Z. Li, "Study of the properties and mechanism of deep reduction and efficient adsorption of Cr(VI) by low-cost $Fe_3O_4$-modified ceramsite," *Science of The Total Environment*, vol. 688, pp. 994–1004, 2019.

[30] Y.-H. Jiang, A.-Y. Li, H. Deng et al., "Characteristics of nitrogen and phosphorus adsorption by Mg-loaded biochar from different feedstocks," *Bioresource Technology*, vol. 276, pp. 183–189, 2019.

[31] P. B. Cusack, M. G. Healy, P. C. Ryan et al., "Enhancement of bauxite residue as a low-cost adsorbent for phosphorus in aqueous solution, using seawater and gypsum treatments," *Journal of Cleaner Production*, vol. 179, pp. 217–224, 2018.

[32] D. Wang, N. Chen, Y. Yu, W. Hu, and C. Feng, "Investigation on the adsorption of phosphorus by Fe-loaded ceramic adsorbent," *Journal of Colloid and Interface Science*, vol. 464, pp. 277–284, 2016.

[33] G. H. Safari, M. Zarrabi, M. Hoseini, H. Kamani, J. Jaafari, and A. H. Mahvi, "Trends of natural and acid-engineered pumice onto phosphorus ions in aquatic environment: adsorbent preparation, characterization, and kinetic and equilibrium modeling," *Desalination and Water Treatment*, vol. 54, no. 11, pp. 3031–3043, 2015.

[34] D. Wang, W. Hu, N. Chen, Y. Yu, C. Tian, and C. Feng, "Removal of phosphorus from aqueous solutions by granular mesoporous ceramic adsorbent based on Hangjin clay," *Desalination and Water Treatment*, vol. 57, no. 47, pp. 22400–22412, 2016.

[35] R. Xie, Y. Chen, T. Cheng, Y. Lai, W. Jiang, and Z. Yang, "Study on an effective industrial waste-based adsorbent for the adsorptive removal of phosphorus from wastewater: equilibrium and kinetics studies," *Water Science and Technology*, vol. 73, no. 8, pp. 1891–1900, 2016.

[36] X. Yuan, C. Bai, W. Xia, B. Xie, and J. An, "Phosphate adsorption characteristics of wasted low-grade iron ore with phosphorus used as natural adsorbent for aqueous solution," *Desalination and Water Treatment*, vol. 54, no. 11, pp. 3020–3030, 2015.

[37] Z. Zhang, Y. Niu, H. Chen et al., "Feasible one-pot sequential synthesis of aminopyridine functionalized magnetic $Fe_3O_4$ hybrids for robust capture of aqueous Hg(II) and Ag(I)," *ACS Sustainable Chemistry & Engineering*, vol. 7, no. 7, pp. 7324–7337, 2019.

[38] X. Song, Y. Niu, Z. Qiu et al., "Adsorption of Hg(II) and Ag(I) from fuel ethanol by silica gel supported sulfur-containing PAMAM dendrimers: kinetics, equilibrium and thermodynamics," *Fuel*, vol. 206, pp. 80–88, 2017.

[39] M. Hanif, R. Nadeem, M. Zafar, K. Akhtar, and H. Bhatti, "Kinetic studies for Ni(II) biosorption from industrial wastewater by Cassia fistula (Golden Shower) biomass," *Journal of Hazardous Materials*, vol. 145, no. 3, pp. 501–505, 2007.

[40] S. Li, T. Lei, F. Jiang et al., "Tuning the morphology and adsorption capacity of Al-MIL-101 analogues with $Fe^{3+}$ for phosphorus removal from water," *Journal of Colloid and Interface Science*, vol. 560, pp. 321–329, 2020.

[41] Q.-x. Jing, Y.-y. Wang, L.-y. Chai et al., "Adsorption of copper ions on porous ceramsite prepared by diatomite and tungsten residue," *Transactions of Nonferrous Metals Society of China*, vol. 28, no. 5, pp. 1053–1060, 2018.

[42] J. Jang and D. S. Lee, "Effective phosphorus removal using chitosan/Ca-organically modified montmorillonite beads in batch and fixed-bed column studies," *Journal of Hazardous Materials*, vol. 375, pp. 9–18, 2019.

[43] K. Y. Koh, S. Zhang, and J. Paul Chen, "Hydrothermally synthesized lanthanum carbonate nanorod for adsorption of phosphorus: material synthesis and optimization, and demonstration of excellent performance," *Chemical Engineering Journal*, vol. 380, p. 122153, 2020.